Synthesis and characterization of ZnO nanowires for nanosensor applications

O. Lupan [a,b,*], G.A. Emelchenko [c], V.V. Ursaki [d,e], G. Chai [a], A.N. Redkin [f], A.N. Gruzintsev [f], I.M. Tiginyanu [d,e,h], L. Chow [a,g], L.K. Ono [a], B. Roldan Cuenya [a,i,j], H. Heinrich [a,g], E.E. Yakimov [f]

[a] Department of Physics, University of Central Florida, Orlando, FL 32816-2385, USA
[b] Department of Microelectronics and Semiconductor Devices, Technical University of Moldova, 168 Stefan cel Mare Blvd., MD-2004 Chisinau, Republic of Moldova
[c] Institute of Solid State Physics, Russian Academy of Science, 142432 Chernogolovka, Moscow District, Russia
[d] Institute of Applied Physics of the Academy of Sciences of Moldova, MD-2028 Chisinau, Republic of Moldova
[e] National Center for Materials Study and Testing, Technical University of Moldova, Chisinau 2004, Republic of Moldova
[f] Institute of Microelectronics Technology and High Purity Materials, Russian Academy of Sciences, 142432 Chernogolovka, Moscow District, Russia
[g] Advanced Materials Processing and Analysis Center, and Department of Mechanical, Materials, and Aerospace Engineering, University of Central Florida, Orlando, FL 32816, USA
[h] Institute of Electronic Engineering and Nanotechnologies, Academy of Sciences of Moldova, MD-2028 Chisinau, Republic of Moldova
[i] Department of Civil, Environmental and Construction Engineering, University of Central Florida, USA
[j] Nanoscience Technology Center, University of Central Florida, Orlando, FL, USA

ARTICLE INFO

ABSTRACT

In this paper we report the synthesis of ZnO nanowires via chemical vapor deposition (CVD) at 650 °C. It will be shown that these nanowires are suitable for sensing applications. ZnO nanowires were grown with diameters ranging from 50 to 200 nm depending on the substrate position in a CVD synthesis reactor and the growth regimes. X-ray diffraction (XRD), scanning electron microscopy (SEM), transmission electron microscopy (TEM), X-ray photoelectron spectroscopy (XPS), photoluminescence (PL), and Raman spectroscopy (RS) have been used to characterize the ZnO nanowires. To investigate the suitability of the CVD synthesized ZnO nanowires for gas sensing applications, a single ZnO nanowire device (50 nm in diameter) was fabricated using a focused ion beam (FIB). The response to H_2 of a gas nanosensor based on an individual ZnO nanowire is also reported.

1. Introduction

In recent years, low-dimensional systems have attracted tremendous research interest for nanosensor applications due to their gas sensitivity, ultraviolet (UV) photoresponse, optical transparency in the visible region, etc. [1–14]. In particular, quasi-one-dimensional (Q1D) nanowires/nanorods are promising as a low-cost material for high-speed UV photoconductive nanoscale detectors and gas sensors [3,7–14].

Current research efforts are focused on the UV light and chemical sensing properties of metal oxide nanowires, such as zinc oxide (ZnO), tin oxide (SnO_2), indium oxide (In_2O_3), aluminum oxide (Al_2O_3), gallium oxide (Ga_2O_3), tungsten oxide (WO_3), and vanadium oxide (V_2O_5) [5,7,15–17]. In particular, several authors have demonstrated that zinc oxide nanowires (NWs) have unique properties, such as high sensitivity under ambient conditions, and that they are a potential candidate for use as a sensing material [7,8,15–17]. In addition, ZnO is a low-cost material which is simple to fabricate, making it attractive for research and industrial applications.

Recently, Tien et al. [18] used Pt-coated ZnO nanorods as sensors capable of detecting ppm concentrations of hydrogen at room temperature. Heo et al. [19] used Au islands for site-selective growth of ZnO nanowires by Molecular Beam Epitaxy (MBE) at 600 °C. Wang et al. [20] studied the response of Pd-coated ZnO nanorods to H_2 at ppm levels in N_2 and found them to be suitable for practical applications in hydrogen selective sensing at room

temperature. In another study by Son et al. [21] ZnO nanowires synthesized by pulsed laser deposition (PLD) were used, and sensitivity to low concentrations of ethanol was reported. ZnO nanorods/nanowires synthesized by different techniques were also reported as sensors of a variety of gases like ammonia, formaldehyde, hydrogen, nitrogen dioxide, and carbon monoxide [7,8,19–25]. According to previous reports the sensitivity of ZnO to gas could be affected by nanostructure, surface defects and post growth annealing in H_2 or O_2 ambient [1,24–28].

At the same time it is necessary to mention that many researchers dealing with the growth of ZnO nanowires use gold nanodrops as a catalyst. Although the ensembles of nanowires obtained in this manner are quite uniform in size, gold is always present as an impurity and alters the crystalline and optical properties of ZnO, possibly affecting also its sensing capabilities and long term stability. Therefore, to improve the emissivity and electrical properties of ZnO nanowires, one has to consider the possibilities of their synthesis without depending on metal catalysts.
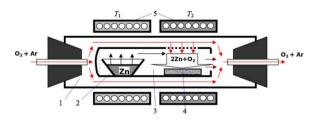
Here, we present the controlled synthesis of ZnO nanowires by chemical vapor deposition (CVD) without the use of a catalyst. In addition, we report details related to the systematic characterization of the as-synthesized zinc oxide nanomaterial for sensor applications. To investigate the sensing properties of the CVD-fabricated ZnO nanowires and their feasibility for nanoscale multifunctional sensor applications, we used a focused ion beam (FIB) set-up to deposit metal electrodes for external contacts. A nanodevice is fabricated from an individual zinc oxide nanowire (50 nm in diameter) and characterized.

2. Experimental details

2.1. Synthesis and nanosensor fabrication

ZnO nanowires were grown on a Si(1 0 0) substrate by the chemical vapor deposition (CVD) procedure at a low pressure (Fig. 1). Metallic zinc of high purity (99.999%) and an oxygen–argon mixture (15 vol.% of oxygen) were the starting reactants [29]. Fig. 1 schematically shows the CVD set-up for the growth of ZnO nanowires on Si substrates. The synthesis was performed in a two-zone quartz flow reactor. In the first zone zinc was evaporated (position 2 in Fig. 1). In the second zone zinc vapors interacted with oxygen. Silicon [(1 0 0)-oriented wafer] substrates were arranged in the second zone (position 4 in Fig. 1). The temperature of zinc evaporation was 670 °C and the growth temperature was 650 °C (second zone in position 4 from Fig. 1). An oxygen–argon mixture was fed to the reactor at a rate of 1 l/h. The consumption of zinc was 20–28 g/h. The synthesis of ZnO nanowires/nanorods proceeded at approximately 30:1 Zn-to-O molar ratio. The pressure in the reactor was maintained at a level of 5 Torr. The synthesis was conducted for 30 min on substrates located at different distances from the zinc source.

Fabrication of an individual ZnO nanowire (50 nm in diameter)-based nanosensor, is described next. First, the ZnO nanowires were

released from the initial substrate by sonication in ethanol. Then, they were transferred to a SiO_2-coated Si substrate cleaned as described in [9,30]. The separated ZnO nanowires were transferred via direct contact with a clean substrate with predeposited Cr/Au external electrodes. Focused Ion Beam (FIB) was used to pattern metal electrodes that contacted both ends of a single ZnO nanowire, as reported elsewhere [7,8,10].

2.2. Characterization

The as-prepared ZnO nanowires on the Si substrate were characterized by X-ray diffraction (XRD) using a Rigaku 'D/B max' X-ray diffractometer (Cu Kα radiation source with λ = 1.54178 Å). The operating conditions were 30 mA and 40 kV at a scanning rate of 0.04°/s. The morphology and chemical composition of the samples were studied using a VEGA TESCAN TS 5130MM scanning electron microscope (SEM) equipped with an Oxford Instruments INCA energy dispersive X-ray (EDX) system. Transmission electron microscopy (TEM) was performed with a FEI Tecnai F30 TEM at an accelerating voltage of 300 kV. To prepare the TEM samples, the nanowires were scraped from the Si substrate onto an amorphous holey carbon film covering a copper TEM grid.
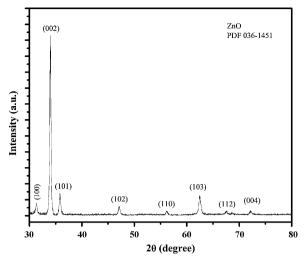
The ex situ prepared samples were mounted on a molybdenum sample holder and subsequently transferred into a modular ultrahigh vacuum (UHV) system (SPECS GmbH) specially designed for the preparation and characterization of nanoscale materials. The X-ray photoelectron spectroscopy (XPS) measurements were conducted in the analysis chamber equipped with a hemispherical electron energy analyzer (Phoibos 100, SPECS GmbH) and a dual-anode (Al Kα, 1486.6 eV and Ag Lα, 2984.4 eV) monochromatic X-ray source (XR50M, SPECS GmbH). For the quantitative analysis of the peak positions and relative spectral areas of the Zn-2p and O-1s components, the raw XPS spectra were fitted with Gaussian–Lorentzian (G–L) functions. The intensity ratio of the Zn-$2p_{3/2}$/2p-$_{1/2}$ spin-orbit doublet was held constant at a value of 2.

The continuous wave (cw) PL was excited by the 351.1 nm line of an Ar$^+$ SpectraPhysics laser and analyzed with a double spectrometer ensuring a spectral resolution better than 0.5 meV. The samples were mounted on the cold station of a LTS-22-C-330 optical cryogenic system. The Raman scattering was investigated at room temperature with a MonoVista CRS Confocal Laser Raman System in the backscattering geometry under the excitation by a 532 nm DPSS laser.

The focused ion beam was employed for the nanoscale sensor fabrication. The gas sensing measurements were performed using an individual ZnO nanowire-based sensor fabricated in the FIB system. The nanosensor was placed in a closed quartz chamber connected to a gas flow system. The concentration of test gases was measured using a pre-calibrated mass flow controller. The test gases were allowed to flow through a pipe network with a diameter of 5 mm to a test chamber with a sensor holder in which the nanosensor was placed [7,8].

3. Results and discussion

ZnO nanowires were synthesized with high yield by controlling the flow rates and partial pressures of oxygen, argon, and zinc vapor at 650 °C. XRD measurements were performed on the ZnO nanowires to assess their structure and phase purity. Fig. 2 displays the XRD spectra of the ZnO nanowires with indexed peaks. It shows that all the nanowires grown on the Si(1 0 0) substrate are pure ZnO with hexagonal structure. No diffraction peaks from metallic Zn or other phases were observed in these samples. The diffraction peaks in the pattern are indexed as the hexagonal wurtzite ZnO structure with lattice constants in accordance with values in the standard card (JCPDS number 36-1451 for ZnO). The measured

Fig. 1. Set-up of chemical vapor deposition for the growth of ZnO nanowires on a Si substrate: (1) flowing quartz reactor, (2) Zn source, (3) internal quartz retort, (4) substrates, (5) electric heaters.
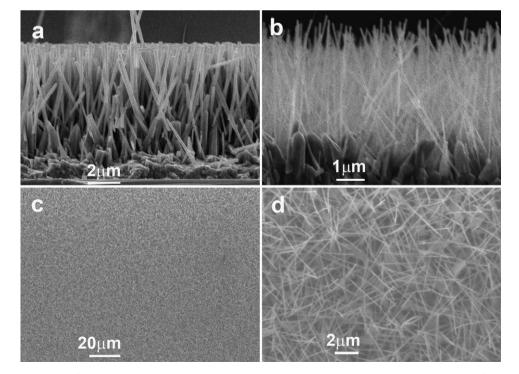
Fig. 2. XRD pattern of ZnO nanowires grown by CVD at 650 °C for 30 min. The indexing of the different XRD peaks was done using as reference a database from the Joint Committee on Powder Diffraction Standards, Powder Diffraction File No 36-1451.

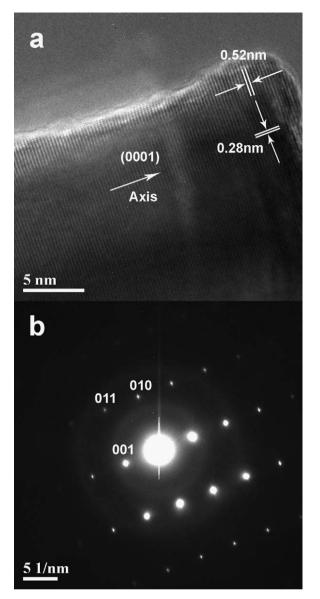lattice parameters of $a = 0.326$ nm and $c = 0.521$ nm are consistent with the standard values.

To see the entire length of ZnO nanowires and whether it is possible to separate each one from another, cross-sectional images of the obtained nanomaterial were acquired. The SEM image in Fig. 3a shows that high densities of 200 nm nanowires grow over the entire ZnO seed layer on the Si substrate positioned at the entrance of the growth zone (higher O/Zn ratio, Fig. 1). It can be seen that a high density of 200 nm nanowires grow over the entire ZnO film predeposited on Si. Fig. 3b shows a cross-sectional SEM view of the samples grown on a Si substrate positioned at the exit zone (lower O/Zn ratio, Fig. 1). Fig. 3c and d shows top-view SEM images of the samples grown on the Si substrate positioned at the exit of the growth zone (position 4 in Fig. 1). Fig. 3c demonstrates

that nanowires grow on the entire surface of the Si substrate. According to the magnified image shown in Fig. 3d, each ZnO nanowire is 50–100 nm in diameter. The average length of the nanowires is about 5–10 μm. These sizes are highly interesting for gas sensing applications.

As suggested by electron microscopy images, Fig. 3a and b, the grown ZnO is a mixture of vertical nanowires/nanorods of different lengths (the length varied from 1 to 20 μm, depending on the position of the silicon substrate in the reactor). The mean diameter of individual nanowires is about 0.05–0.25 μm and crystal faceting is fairly well developed. The following peculiarities were observed in the ZnO nanowires/nanorods growth: (1) growth of vertical NWs started for a certain critical ratio of oxygen/zinc vapors R_c; for $R < R_c$, we observed the growth of randomly oriented nanowires/nanorods, (2) a morphological transition from a nanorod shape to a nanoribbon shape (not shown) is observed for a larger temperature difference of about 80 K between the evaporation zone and deposition zone. Fig. 3 demonstrates the first peculiarity: Fig. 3a presents ZnO nanocrystals grown at the entrance zone and Fig. 3b shows ZnO nanocrystals grown at the exit zone. The shape and the size of the ZnO nanowires/nanorods were found to depend on the position of the substrate in the growth zone.

To study the as-synthesized ZnO nanowires, transmission electron microscopy (TEM) was employed. Fig. 4a shows the high-resolution transmission electron microscopy (HRTEM) image of a ZnO nanowire grown by CVD. Fig. 4b presents a selected area electron diffraction (SAED) pattern of a ZnO nanowire grown by CVD. SAED pattern and HRTEM image reveal that the ZnO nanowires are uniform and have single crystal structure. As indexed in the SAED pattern, the nanowire is grown along the direction of the c-axis of ZnO, in agreement with the HRTEM result. The HRTEM image indicates that the entire as-grown ZnO nanowire has crystalline wurtzite structure grown along the [0 0 1] direction, which is consistent with the XRD results. Fig. 4 reveals that, in this region, the nanowire possesses a crystal structure without dislocations and stacking faults.
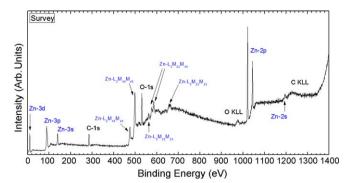

Fig. 3. SEM images of the cross-section of ZnO nanowire arrays with respect to the substrate position in the growth zone: (a) at the entrance of the growth zone (ratio O/Zn is larger), (b) at the exit of the growth zone (ratio O/Zn is smaller). Next are the SEM top-view images: (c) of the ZnO nanowires grown on ZnO/Si placed at the exit of zone (ratio O/Zn is smaller), (d) zoom in view image of the ZnO nanowires.

Fig. 5. Survey XPS spectrum corresponding to ZnO nanowires supported on SiO₂/Si(0 0 1). Only Zn, O and adventitious C (from sample transport in air) are detected. The different photoelectron and Auger electron peaks (AES) peaks observed for the latter elements are labeled in the graph.

Fig. 5 shows a survey XPS spectrum from the pure ZnO nanowires indicating the presence of the following elements: Zn, O and adventitious C. No contaminants from the ZnO nanowire synthesis were detected on the sample surface. The XPS spectra of the (a) Zn-2p and (b) O-1s core level regions of our sample can be seen in Fig. 6. The ZnO nanowires display a doublet at 1021.4 and 1044.5 eV (vertical reference lines) corresponding to the Zn-$2p_{3/2}$ and $2p_{1/2}$ core levels [35,36]. The linewidths observed (FWHM = 1.7 eV) are in agreement with previous data acquired on pure ZnO nanorods [17,31]. The asymmetric peak observed in the O-1s region, Fig. 6b, was deconvoluted by four subspectral components: (i) ZnO (530.2 eV, 63% spectral area, solid line), (ii) defective ZnO_x (531.6 eV, 21%, dashed line), (iii) adventitious CO (531.1 eV, 6%, dotted line) [37], and (iv) adventitious CO_2 (532.5 eV, 10%, dashed-dotted line) [38,39]. Armelao et al. [43] and Liqiang et al. [44] observed similar components in their O-1s

Fig. 6. XPS spectra (Al Kα = 1486.6 eV) corresponding to the (a) Zn-2p and (b) O-1s core level regions of ZnO nanowires supported on SiO₂/Si(0 0 1).

Fig. 4. (a) HRTEM image of ZnO nanowire grown by CVD method and (b) its corresponding selected area electron diffraction SAED pattern.
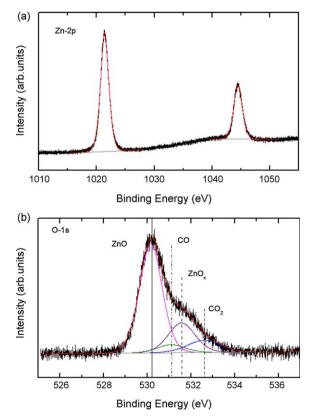
The EDX analysis of the produced structures demonstrates a stoichiometric ZnO composition (within a precision of 1 at.%). The characterization confirmed that the nanowire arrays are highly crystalline, regular and distributed throughout the substrate surface.

XPS was used to characterize the composition of pure ZnO nanowires and to investigate whether any undesirable chemical residues from our synthetic route remained on the sample surface. Positive binding energy (BE) shifts were observed in the XPS spectra due to sample charging. Therefore, the BE scale was calibrated using the adventitious carbon peak (C-1s) at 285 eV as in Refs. [17,31]. In our samples, residual amounts of adventitious carbon and carbonyl compounds are unavoidable due to their exposure to air prior to the XPS analysis [32]. In addition to the adventitious carbon peak, the C-1s XPS spectrum of our samples (not shown) also displays two additional peaks at 286.6 and 288.7 eV corresponding to C=O and O=C–O, respectively [32–34]. As will be described below, those peaks were also used as reference in the determination of the different O species present in our samples.
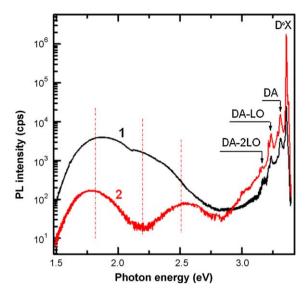
Fig. 7. Emission spectra of the ZnO nanowires with diameters of 50 nm (1) and 200 nm (2). T = 10 K.

Fig. 8. The neutral donor- and free-exciton lines in the luminescence (1) and reflectivity (2) spectra of ZnO layers grown by CVD. T = 10 K.

spectra and attributed the high BE peak to Zn–OH species. Considering their O-1s/Zn-2p XPS intensity ratios, a $ZnO_x(OH)_y$ stoichiometry was suggested [43]. In our studies, the total O-1s/Zn-2p ratio was found to be 1.7 ± 0.2. Thus, the 531.6 eV component could be attributed to the presence of partially reduced ZnO (ZnO_x) [40–42] or ZnOH [43,44].

It is known that point defects in zinc oxide strongly influence the electrical properties which are extremely important for the gas sensor applications. For instance, ZnO with a high density of oxygen vacancies has been shown to have a high electrical conductivity [45]. According to previous theoretical predictions the surface defects such as oxygen vacancies can dominate the electronic/chemical properties and adsorption behaviors of metal oxide surfaces [46,47]. To reveal the presence of deep levels (DL) in ZnO nanowires we compare the intensities of the visible and ultraviolet (UV) luminescence.
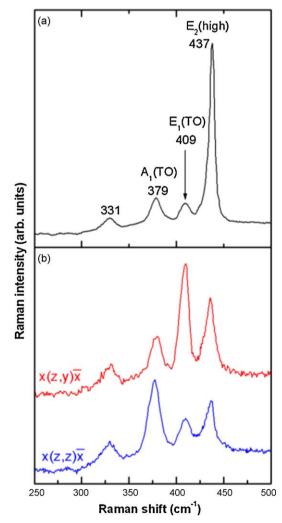
Fig. 7 displays the photoluminescence (PL) spectra of the ZnO nanowires with diameters of 50 nm and 200 nm. Usually zinc oxide exhibits an ultraviolet emission (at about 380 nm at room temperature) due to near band edge electron transition [48,49]. The low temperature spectrum of the near band edge emission is dominated by the excitonic luminescence in the nanowires independently of diameter. However, the ratio of the intensity of excitonic emission to the donor acceptor pair recombination (DA) emission varies from 7 to more than 200 upon increasing the nanowire diameter from 50 nm to 200 nm (Fig. 7). The origin of the DA luminescence band has been previously investigated in detail [50].

The intensity of the near band edge luminescence is around four orders of magnitude higher as compared to the visible emission of the nanowires with a diameter of 200 nm. At the same time, the ratio of the intensity of the near band edge luminescence to the intensity of the visible emission is only around 6 for nanowires with a 50 nm diameter. The visible emission is a combination of a red (~1.8 eV), a yellow (~2.2 eV), and a green (~2.5 eV) PL bands. Usually, the visible emission from ZnO is attributed to different defects such as oxygen vacancies (V_O), zinc vacancies (V_{Zn}) or a complex defect involving interstitial zinc (Zn_i) and interstitial oxygen (O_i) [48,49,51]. The extremely low intensity of the visible emission as compared to the near band edge emission in nanowires with a diameter of 200 nm is an indication of low defect concentration. However, the concentration of defects is strongly dependent on the nanowire diameter.

The optical quality of the produced ZnO nanowires is indicated also by the presence of the free-exciton (FX) luminescence in the emission spectra as evidenced from the analysis of the near band edge PL spectrum of ZnO nanowires in combination with the

Fig. 9. Room temperature micro-Raman spectra of the ZnO nanowires: (a) non-polarized Raman spectrum measured in the quasi-backscattering geometry in the region of the TO phonons. (b) The polarized Raman spectra measured in-plane, i.e. from the edge of the sample (in the x-direction).

reflectivity spectrum of a smooth ZnO layer produced by CVD (Fig. 8). The PL and the reflectivity spectra are superimposed on the same graph. The ground states of the free A and B excitons in the reflectivity spectra are in good agreement with the two PL bands in the high-energy region of the donor-bound exciton lines. The neutral donor exciton lines (D^0X) are identified as the previously reported I_1, I_4, and I_6 lines [52].

Fig. 9 shows the room temperature micro-Raman spectra of the ZnO NWs grown on a ZnO/Si template. The Raman scattering study also demonstrates the high crystallinity of the produced nanowires. The non-polarized Raman spectrum measured in the quasi-backscattering geometry in the region of the transverse optical (TO) phonons in the out plane of the sample surface, i.e. in the z-direction, is illustrated in Fig. 9a. Apart from the $A_1(TO)$, $E_1(TO)$ and E_2(high) modes, a peak at 331 cm^{-1} is observed in the spectrum which is attributed to second order Raman processes involving acoustic phonons [53]. The peak corresponding to the E_2(high) mode has a linewidth of about 6 cm^{-1} which is comparable to values reported for high quality ZnO bulk crystals [54]. The position of the E_2 (high) peak corresponds to the phonon of a bulk ZnO crystal [54] indicating a strain-free state of the nanowire. The polarized Raman spectra measured in-plane, i.e. from the edge of the sample (in the x-direction), are shown in Fig. 9b.

One can see that in the (z,y) polarization for which the $E_1(TO)$ is allowed and the $A_1(TO)$ is forbidden, the intensity of the $E_1(TO)$ phonon is a factor of 3 higher than the $A_1(TO)$ phonon. An inverse ratio is observed for the (z,z) polarization for which the $A_1(TO)$ is allowed and the $E_1(TO)$ is forbidden. Thus, the Raman scattering study demonstrates the high crystalline quality of the nanowires and their predominant orientation perpendicular to the substrate surface.

An SEM image of the transferred ZnO nanowires is shown in Fig. 10. The nanosensor fabricated from an individual ZnO nanowire with patterned metal electrodes contacting both ends is shown in Fig. 10. The current–voltage curves (not included) show a linear behavior, which is very important for sensing applications. For gas-sensing studies, a nanosensor was mounted in a measuring apparatus consisting of a closed quartz chamber connected to a gas flow system. The concentration of test gases was controlled using a pre-calibrated mass flow controller [7,8]. Fig. 11 shows the H_2 gas responses (in %) of a single nanowire ZnO sensor with a concentration of 100 ppm of H_2 in air. For the ZnO nanowire-based sensor the response increased rapidly after gas was introduced into

Fig. 11. Gas-response curve of the individual zinc oxide nanowire-based gas nanosensor under exposure to 100 ppm of H_2 gas at room temperature.

the measurement chamber. The 90% gas response time ($|t_{10\%} - t_{90\%\,in\,H_2}|$) and recovery time ($|t_{90\%\,in\,H_2} - t_{10\%}|$) under exposure to 100 ppm of H_2 at room temperature were determined from Fig. 11. The ($|t_{10\%} - t_{90\%\,in\,H_2}|$) is about 60 s and ($|t_{90\%\,in\,H_2} - t_{10\%}|$) is around 10 s. It should be noted that the H_2 gas response of this ZnO nanowire sensor is about 10 times higher than our previous measurements of ZnO nanorods sensors [7,8]. This could be attributed to the nanowire's higher surface to volume ratio and its superior quality according to all charactersitics described above.

The obtained results demonstrate that CVD-grown ZnO nanowires can be used as sensing material in nanosensors. An individual nanowire-based sensor can have a 30–35% response to 100 ppm of H_2 at room temperature. Measurements are reproducible with time and several working nanodevices fabricated from CVD ZnO nanowires have been measured. By using the developed sensor structure one can avoid operating at high temperature to achieve the desired gas response, especially in hazardous and explosive atmospheres. Another strong argument is that the demonstrated structure can operate at room temperature in a H_2 medium. In this way changes of the ZnO nanowire parameters with time can be avoided. This is important due to the fact that H_2 strongly affects electrical characteristics of ZnO material even if it is exposed at 200 °C as it was demonstrated in other works [55–58]. Thus, by working at room temperature one can avoid functioning at high temperatures in the presence of hydrogen gas, which can act as an unintentional donor and at the same time is an explosive gas.

4. Conclusions

We have developed a CVD technique to grow high quality ZnO nanowires with diameters ranging from 50 to 200 nm. Through the control of the oxygen/zinc ratio, vertically aligned nanowires have been grown. The shape and the size of the ZnO nanorods were found to depend on the position of the substrate in the growth zone. This dependence is explained by rapid oxygen consumption in the reaction zone. The structural and chemical (stoichiometric) quality of the ZnO nanowires was verified through SEM, HRTEM, XPS, Raman and PL measurements. The obtained nanowires are transferable to another substrate with prepatterned external contacts. A single ZnO nanosensor was fabricated using a FIB set-up. FIB lithography was used to pattern metal electrodes contacting both ends of a single ZnO nanowire. The individual ZnO nanowires can be used as a sensing material in nanosensors with a higher response to hydrogen gas at room temperature in comparison with previous reports [7,8,59].
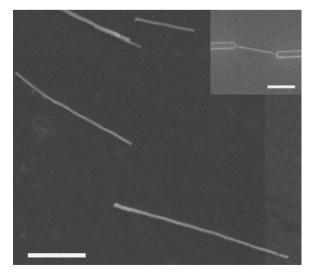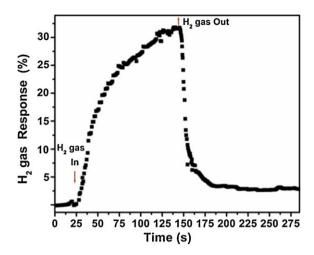

Fig. 10. Scanning electron micrograph of transferred ZnO nanowires. The insert shows device based on a single nanowire of 50 nm in diameter. Scale bars are 2 μm.

Acknowledgements

References

[1] Y.W. Heo, D.P. Norton, L.C. Tien, Y. Kwon, B.S. Kang, F. Ren, S.J. Pearton, J.R. LaRoche, Mater. Sci. Eng.: R: Rep. 47 (2004) 1.
[2] Q.H. Li, Y.X. Liang, Q. Wan, T.H. Wang, Appl. Phys. Lett. 85 (2004) 6389.
[3] C. Soci, A. Zhang, B. Xiang, S.A. Dayeh, D.P.R. Aplin, J. Park, X.Y. Bao, Y.H. Lo, D. Wang, Nano Lett. 7 (2007) 1003.
[4] L. Chow, O. Lupan, H. Heinrich, G. Chai, Appl. Phys. Lett. 94 (2009) 163105.
[5] O. Lupan, L. Chow, G. Chai, A. Schulte, S. Park, H. Heinrich, Mater. Sci. Eng. B 157 (2009) 101.
[6] O. Lupan, L. Chow, G. Chai, H. Heinrich, S. Park, A. Schulte, J. Cryst. Growth 311 (2008) 152.
[7] O. Lupan, L. Chow, G. Chai, Microelectron. Eng. 85 (2008) 2220.
[8] O. Lupan, G. Chai, L. Chow, Microelectron. J. 38 (2007) 1211.
[9] G. Chai, O. Lupan, L. Chow, H. Heinrich, Sens. Actuators A: Phys. 150 (2009) 184.
[10] O. Lupan, L. Chow, G. Chai, L. Chernyak, O. Lopatiuk-Tirpak, H. Heinrich, Phys. Stat. Sol. (a) 205 (2008) 2673.
[11] J. Suehiro, N. Nakagawa, S. Hidaka, M. Ueda, K. Imasaka, M. Higashihata, T. Okada, M. Hara, Nanotechnology 17 (2006) 2567.
[12] M. Law, D.J. Sirbuly, J.C. Johnson, J. Goldberger, R.J. Saykally, P. Yang, Science 305 (2004) 1269.
[13] Q.H. Li, Q. Wan, Y.X. Liang, T.H. Wang, Appl. Phys. Lett. 84 (2004) 4556.
[14] X.D. Bai, P.X. Gao, Z.L. Wang, E.G. Wang, Appl. Phys. Lett. 82 (2003) 4806.
[15] A. Kolmakov, M. Moskovits, Annu. Rev. Mater. Res. 34 (2004) 151.
[16] Z.L. Wang, J. Phys.: Condens. Mat. 16 (2004) R829.
[17] O. Lupan, L. Chow, G. Chai, B. Roldan Cuenya, A. Naitabdi, A. Schulte, H. Heinrich, Mater. Sci. Eng. B 145 (2007) 57.
[18] L.C. Tien, P.W. Sadik, D.P. Norton, L.F. Voss, S.J. Pearton, H.T. Wang, B.S. Kang, F. Ren, J. Jun, J. Lin, Appl. Phys. Lett. 87 (2005) 222106.
[19] Y.W. Heo, V. Varadarajan, M. Kaufman, K. Kim, D.P. Norton, F. Ren, P.H. Fleming, Appl. Phys. Lett. 81 (2002) 3046.
[20] H.T. Wang, B.S. Kang, F. Ren, L.C. Tien, P.W. Sadik, D.P. Norton, S.J. Pearton, J. Lin, Appl. Phys. Lett. 86 (2005) 243503.
[21] J.Y. Son, S.J. Lim, J.H. Cho, W.K. Seong, H. Kim, Appl. Phys. Lett. 93 (2008) 053109.
[22] J.B.K. Law, J.T.L. Thong, Nanotechnology 19 (2008) 205502.
[23] L. Peng, Q. Zhao, D. Wang, J. Zhai, P. Wang, S. Pang, T. Xie, Sens. Actuators B 136 (2009) 80.
[24] M.W. Ahn, K.S. Park, J.H. Heo, J.G. Park, D.W. Kim, K.J. Choi, J.H. Lee, S.H. Hong, Appl. Phys. Lett. 93 (2008) 263103.
[25] L. Liao, H.B. Lu, M. Shuai, J.C. Li, Y.L. Liu, C. Liu, Z.X. Shen, T. Yu, Nanotechnology 19 (2009) 175501.
[26] L. Liao, H.B. Lu, J.C. Li, C. Liu, D.J. Fu, Y.L. Liu, Appl. Phys. Lett. 91 (2007) 173110.
[27] I.L. Lyubchanskii, N.N. Dadoenkova, M.I. Lyubchanskii, E.A. Shapovalov, A. Lakhtakia, Th. Rasing, Appl. Phys. Lett. 85 (2004) 5932.
[28] Y. Zhang, A. Kolmakov, S. Chretien, H. Metiu, M. Moskovits, Nano Lett. 4 (2004) 403.
[29] A.N. Redkin, Z.I. Makovei, A.N. Gruzintsev, S.V. Dubonos, E.E. Yakimov, Inorg. Mater. 43 (2007) 253.
[30] S.T. Shishiyanu, O.I. Lupan, T.S. Shishiyanu, V.P. Şontea, S.K. Railean, Electrochim. Acta 49 (2004) 4433.
[31] V.I. Nefedov, Y.V. Salyn, G. Leonhardt, R. Scheibe, J. Electron Spectrosc. Relat. Phenom. 10 (1977) 121.
[32] K. Kawase, J. Tanimura, H. Kurokawa, K. Wakao, M. Inone, H. Umeda, A. Teramoto, J. Electrochem. Soc. 152 (2005) G163.
[33] O. Joubert, J. Pelletier, C. Fiori, T.A.N. Tan, J. Appl. Phys. 67 (1990) 4291.
[34] W.R. Salaneck, A. Paton, D.T. Clark, J. Appl. Phys. 47 (1976) 144.
[35] NIST X-ray Photoelectron Spectroscopy Database, version 3.5, http://srdata.nist.gov/xps/.
[36] B.R. Strohmeier, D.M. Hercules, J. Catal. 86 (1984) 266.
[37] K. Tanaka, K. Miyahara, I. Toyoshima, J. Phys. Chem. 88 (1984) 3504.
[38] A.F. Carley, G. Hawkins, S. Read, M.W. Roberts, Top. Catal. 8 (1999) 243.
[39] H. Onishi, C. Egawa, T. Aruga, Y. Iwasawa, Surf. Sci. 191 (1987) 479.
[40] Y. Tak, D. Park, K.J. Yong, J. Vac. Sci. Technol. B 24 (2006) 2047.
[41] X.J. Yang, X.Y. Miao, X.L. Xu, C.M. Xu, J. Xu, H.T. Liu, Opt. Mater. 27 (2005) 1602.
[42] M. Chen, X. Wang, Y.H. Yu, Z.L. Pei, X.D. Bai, C. Sun, R.F. Huang, L.S. Wen, Appl. Surf. Sci. 158 (2000) 134.
[43] L. Armelao, M. Fabrizio, S. Gialanella, F. Zordan, Thin Solid Films 394 (2001) 89.
[44] O. Lupan, T. Pauporté, L. Chow, B. Viana, F. Pellé, L.K. Ono, B. Roldan Cuenya, H. Heinrich, Effects of annealing on properties of ZnO thin films prepared by electrochemical deposition in chloride medium, Appl. Surf. Sci. 256 (2010) 1895; J. Liqiang, W. Dejun, W. Baiqi, L. Shudan, X. Baifu, F. Honggang, S. Jiazhong, J. Mol. Catal. A 244 (2006) 193.
[45] P.C. Chang, Z. Fan, D. Wang, W.Y. Tseng, W.A. Chiou, J. Hong, J.G. Liu, Chem. Mater. 16 (2004) 5133.
[46] V.E. Henrich, P.A. Cox, The Surface Science and Metal Oxides, Cambridge University Press, Cambridge, 1994.
[47] R. Schaub, E. Wahlstrom, A. Ronnaus, E. Laegsgaard, I. Stensgaard, F. Besenbacher, Science 299 (2003) 377.
[48] Ü. Özgür, Ya.I. Alivov, C. Liu, A. Teke, M.A. Reshchikov, S. Dogan, V. Avrutin, S.J. Cho, H. Morkoç, J. Appl. Phys. 98 (2005) 041301.
[49] H.C. Ong, G.T. Du, J. Cryst. Growth 265 (2004) 471.
[50] V.V. Ursaki, I.M. Tiginyanu, V.V. Zalamai, V.M. Masalov, E.N. Samarov, G.A. Emelcenko, F. Briones, Semicond. Sci. Technol. 19 (2004) 851.
[51] A.B. Djurisic, Y.H. Leung, K.H. Tam, Y.F. Hsu, L. Ding, W.K. Ge, Y.C. Zhong, K.S. Wong, W.K. Chan, H.L. Tam, K.W. Cheah, W.M. Kwok, D.L. Phillips, Nanotechnology 18 (2007) 095702.
[52] B.K. Meyer, H. Alves, D.M. Hofmann, W.D. Kriegseis, F. Forster, J. Bertram, A. Christen, M. Hoffmann, M. Straßburg, U. Dworzak, A.V. Haboeck, Rodina, Phys. Stat. Sol. (b) 241 (2004) 231.
[53] M. Rajalakshmi, A.K. Arora, B.S. Bendre, S. Mahamuni, J. Appl. Phys. 87 (2000) 2445.
[54] J. Serrano, F.G. Manjon, A.H. Romero, F. Widulle, R. Lauck, M. Cardona, Phys. Rev. Lett. 90 (2003) 055510.
[55] E. Mollwo, Z. Phys. 138 (1954) 478.
[56] S.J. Baik, J.H. Jang, C.H. Lee, W.Y. Cho, K.S. Lim, Appl. Phys. Lett. 70 (1997) 3516.
[57] S. Kohiki, M. Nishitani, T. Wada, T. Hirao, Appl. Phys. Lett. 64 (1994) 2876.
[58] O. Lupan, V.V. Ursaki, G. Chai, L. Chow, G.A. Emelchenko, I.M. Tiginyanu, A.N. Gruzintsev, A.N. Redkin, Sens. Actuators B: Chem. 144 (1) (2010) 56.
[59] O. Lupan, G. Chai, L. Chow, Sens. Actuators B: Chem. 141 (2009) 511.